PERGAMON

International Journal of Solids and Structures 38 (2001) 7839–7856

INTERNATIONAL JOURNAL OF SOLIDS and STRUCTURES

www.elsevier.com/locate/ijsolstr

Influence of elastic gradient profiles on dynamically loaded functionally graded materials: cracks along the gradient

C.-E. Rousseau, H.V. Tippur *

Department of Mechanical Engineering, Auburn University, 202 Ross Hall, Auburn, AL 36849, USA

Received 1 October 2000; in revised form 1 May 2001

Abstract

The effect of different elastic gradient profiles on the fracture behavior of dynamically loaded functionally graded materials (FGM) having cracks parallel to the elastic gradient is studied numerically. Finite element analyses of FGM and homogeneous beams are used to examine crack tip responses to low velocity, symmetric impact loading on the uncracked edge of the beams. Elastic description of FGMs consist of unidirectional power-law variation of E/ρ and constant Poisson's ratio. The results show the effect of the variations in elastic profiles to be relatively small for cases with cracks residing on the stiff side of the FGM whereas significant differences are seen when cracks are on the compliant side. Elastic property variations also affect crack tip loading rate and hence crack initiation in FGMs. Crack initiation in FGMs with cracks on the stiff side are significantly delayed due to a lower rate of crack tip loading when compared to the opposite configuration or the equivalent homogeneous materials.

Keywords: Functionally graded materials; Material nonhomogeneity; Finite element modeling; Stress intensity factors; Dynamic fracture

1. Introduction

Functionally graded materials (FGMs) are known to offer significant advantages over discretely layered material systems. Gradual variation of material composition instead of abrupt changes is known to be beneficial for improving failure performance while preserving the intended thermal, tribological, and/or structural benefits of combining dissimilar materials. FGMs are considered ideal candidates for applications involving high strain rate and thermal shock loading. Assessing the influence of compositional and hence material property gradients on dynamic failure behavior is central to understanding FGMs. In this article, the influence of different elastic gradient profiles on dynamic fracture behavior of FGMs is examined numerically.

At the moment, studies on dynamic fracture of FGMs are rather scarce. Delale and Erdogan (1983) were among the first to analyze the behavior of FGMs under quasi-static loading conditions. Eischen (1987), Jin

* Corresponding author. Tel.: +1-334-844-3327; fax: +1-334-844-3307.
E-mail address: htippur@eng.auburn.edu (H.V. Tippur).

0020-7683/01/$ - see front matter
PII: S0020-7683(01)00127-5

and Noda (1994), and Erdogan (1995) have established the retention of the square root stress singularity at the crack tip as in homogeneous materials for static loading. Dynamic stress intensity factors (SIF) for a mode-III crack lying in an elastic media with spatially varying elastic properties normal to crack surfaces has been studied analytically by Babaei and Lukasiewicz (1998). They have found SIF to vary with crack length to layer thickness ratio. Dynamic crack propagation in functionally graded particle dispersed material is numerically studied by Nakagaki et al. (1998) for shock loading to determine the effect of grading on crack severity as the crack propagates in the FGM. Parameswaran and Shukla (1998) have shown experimentally that increasing toughness in the direction of crack growth reduces crack jump distance in discretely layered FGMs. Chiu and Erdogan (1999) have evaluated the effect of material nonhomogeneity on one-dimensional wave propagation in FGMs having gradation in the direction of the incident pulse. Considerable wave distortions are reported as a rectangular pressure pulse propagates in the material. Parameswaran and Shukla (1999) have performed asymptotic analysis to establish equations describing stress fields around steadily growing cracks along the elastic gradient of FGMs. They have obtained explicit expressions for the sum of in-plane normal stresses and nonhomogeneity specific higher order terms. Finally, Marur and Tippur (2000) have used a hybrid strain gage measurements and numerical simulations to evaluate dynamic performance of graded interface having cracks normal to the elastic gradient with respect to those of bimaterial. They have measured lower rate of crack tip loading in FGMs compared to the bimaterial counterparts.

Numerical evaluation of cracked FGMs with cracks oriented along the material gradient is also limited. Eischen (1987) modified the standard domain integral for FGMs with cracks oriented in the direction of the gradient. He developed a path independent integral J^* pertinent to non-homogeneous materials and asserted its validity by applying it to finite element simulations of several FGM plates with central and edge cracks. Tohgo et al. (1996) have used finite element analysis to show that SIF and plastic zone at the FGM crack is affected by the mechanical properties of the gradient. Kim et al. (1997) have evaluated the effects of plasticity at the tip of a crack approaching the interface of an FGM and a homogeneous material. Li et al. (1999) have investigated crack growth in a UV irradiated polymeric sheet with a small Young's modulus gradient. They have measured far-field loads and used them to numerically evaluate crack growth resistance behavior along the gradient direction. Rousseau and Tippur (2000a) have performed finite element analyses in conjunction with experiments to determine the effect of crack location on the performance of FGMs when the crack is perpendicular to the elastic gradient. Finally, Gu et al. (1999) have used finite element simulations to establish a limit within which the standard domain integral may be applied to non-homogeneous materials.

In the present study, the influence of different unidirectional elastic profiles in FGMs subjected to low velocity impact is studied when cracks are oriented parallel to the direction of the elastic gradient. This evaluation is a step towards tailoring the elastic gradients in FGMs for impact loading conditions. Following this introduction, a brief description of the stress fields present about the crack tip of FGMs is given. Section 3 describes the numerical simulations performed in this study. Section 4 provides the development and equations defining various gradient profiles. Finally, Section 5 presents results of the numerical comparison between FGMs with various gradient profiles, subjected to dynamic impact.

2. Crack tip fields in functionally graded materials: background

2.1. Quasi-statically loaded crack

Jin and Noda (1994) have predicted that, independent of the orientation of a crack with respect to the elastic gradient in an FGM, K-dominant stress fields are free of the influence of the gradient. Thus, under static conditions, tractions at the crack tip in an FGM are described as:

$$\sigma_{ij}(r,\theta) \cong \frac{K_{\mathrm{I}}}{\sqrt{2\pi r}} f_{ij}^{\mathrm{I}}(\theta) + O(r^{1/2}), \quad (i,j = x,y), \tag{1}$$

where K_{I} is the mode-I SIF, and r and θ are the crack tip polar coordinates. Functions f_{ij}^{I} are the angular functions identical to those present in the description of homogeneous crack tip behavior. Higher order description of crack tip tractions as an asymptotic expansion shows (Eischen, 1987) the coefficients of $r^{-1/2}$, and r^0 to also be identical to those present in the asymptotic formulation of homogeneous crack tip behavior. Only terms of order $r^{1/2}$ and beyond would be influenced by the gradient, thereby have coefficients differing from those of homogeneous materials. However, those are yet to be determined.

Delale and Erdogan (1983) have developed near tip expressions for stress fields in non-homogeneous planar bodies that include the influence of elastic property gradients. For an exponential variation of elastic modulus of the form,

$$E(x) = E_0 \mathrm{e}^{\alpha x} = E_0 \mathrm{e}^{r\alpha\cos\theta}, \tag{2}$$

where E_0 is the Young's modulus at the origin, and α is a scalar dependent on the terminal values of the modulus and the length of the graded region, the near tip mode-I stresses are shown to be of the form (Erdogan, 1995),

$$\sigma_{ij}(r,\theta) \cong \mathrm{e}^{r\alpha\cos\theta}\left(\frac{K_{\mathrm{I}}}{\sqrt{2\pi r}} f_{ij}^{\mathrm{I}}(\theta)\right), \quad (i,j = x,y). \tag{3}$$

As $r \to 0$, Eq. (3) reduces to the K-dominant terms of Eq. (1).

2.2. Dynamically propagating crack

Analysis of dynamically propagating cracks in FGMs has been very limited. Thus far to the authors' knowledge, only Parameswaran and Shukla (1999) have described crack tip stresses near dynamically propagating mode-I and mode-II cracks in FGMs. They have derived equations for steadily propagating cracks along the gradient in FGMs with linearly or exponentially varying shear moduli. These solutions correspond to specialized materials with constant ρ or constant E/ρ ratio.

Recently, Rousseau and Tippur (2001a) have demonstrated, experimentally and numerically, the adequacy of the first few homogeneous terms in describing FGM quasi-static crack tip stress fields in cases where the elastic gradient varies moderately (ratio of terminal Young's modulus E values of 3 to 1 over 20 mm). In the absence of a definite stress field for dynamically loaded stationary crack, it is inferred here that the asymptotic equation derived for statically loaded FGMs (Eq. (1)) will also perform adequately for dynamic cases where inertial effects enter the coefficients without modifying the form of the expressions.

3. Computational model

Computational models used in this study simulated dynamic experiments on glass-filled epoxy FGMs that were carried out by Rousseau and Tippur (2001b) in a one-point symmetric impact loading configuration. They involved FGMs with terminal dynamic Young's modulus values at the bottom and top edges having ratios of 3 to 1 along the height of the beam. Material properties did not vary through the thickness or along the length of the FGM. Geometry and loading configuration of the FGM are shown in Fig. 1. Note that for any FGM configuration, E_2 designates the elastic modulus at the top or impact edge, whereas E_1 is the modulus at the bottom or cracked edge. Therefore, FGMs for which $E_2/E_1 < 1$ have a crack on the stiff side of the material while being impacted on the compliant side. On the other hand, FGMs with $E_2/E_1 > 1$ have a crack on the compliant side and are impacted on the stiff side. Materials with $E_2/E_1 = 1$

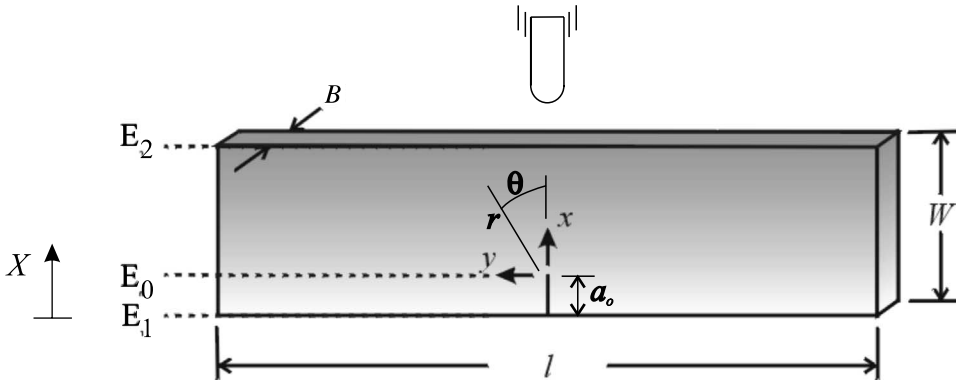

Fig. 1. Configuration of FGM specimens.

are homogeneous. Here, symbol E_0 is used to denote the local value of the crack tip modulus. Material density at these three locations is noted by ρ with the respective subscripts.

The plane stress, elasto-dynamic finite element analyses were performed for both homogeneous and FGM beams. The numerical simulations were carried-out using two-dimensional eight-noded isoparametric quadrilateral elements with two degrees of freedom per node. Because of symmetry, only half of the specimens were modeled, as shown in Fig. 2. The beams were subjected to one point impact loading by a rigid impactor with cylindrical contact profile. Therefore, the only external boundary condition imposed on the model was displacement of the topmost node situated on the crack plane at the rate equal to the impact velocity. Also, along the centerline, at the uncracked ligament, symmetric boundary conditions were imposed. No special crack tip elements were used in the model such as not to pre-suppose any singularity at the FGM crack tip. The Newmark time-integration scheme was used with a minimum time step of 0.04 μs. The results were post-processed every 5 μs.

Implementation of material properties for the homogeneous materials in finite element analyses is routine. However, it is more intricate in the case of FGMs since material properties vary continuously, requiring specification of properties, say, for each row of element along the height of the beam. A scheme was devised to provide easier implementation of the gradient, and a more accurate variation of material property within the element. This was accomplished as follows:

Consider a rectangular homogeneous isotropic continuum having thermal conductivity k, and uniform initial temperature T. Let the two vertical edges be insulated and the top and bottom horizontal faces be disturbed by ambient temperatures T_t and T_b, respectively. If both horizontal faces have the same arbitrary heat transfer coefficient, h, the system will reach steady state and the bulk of the material will have a linear temperature gradient varying from T_b at the bottom edge to T_t, at the top edge (see schematic in Fig. 2). Upon discretizing the domain into finite elements and solving the governing equation for steady state heat flow subjected to the boundary conditions enumerated above, a linear temperature variation will ensue, varying from node to node in the vertical direction, while remaining constant along any horizontal set of nodes. Applying these temperatures as boundary conditions in a structural model, and defining material properties to be functions of temperature, these properties are thus set to follow the established temperature variation. If non-linear material properties are to be applied, heat generation rates are also introduced at strategic locations through the model to achieve such a variation. Young's moduli, Poisson's ratios, and densities were thus established in the finite element model of the FGM. Material properties having been set, unwanted thermal stresses generated by the temperature variations through the model must be eliminated. This is accomplished be setting the coefficient of thermal expansion, α, to zero.

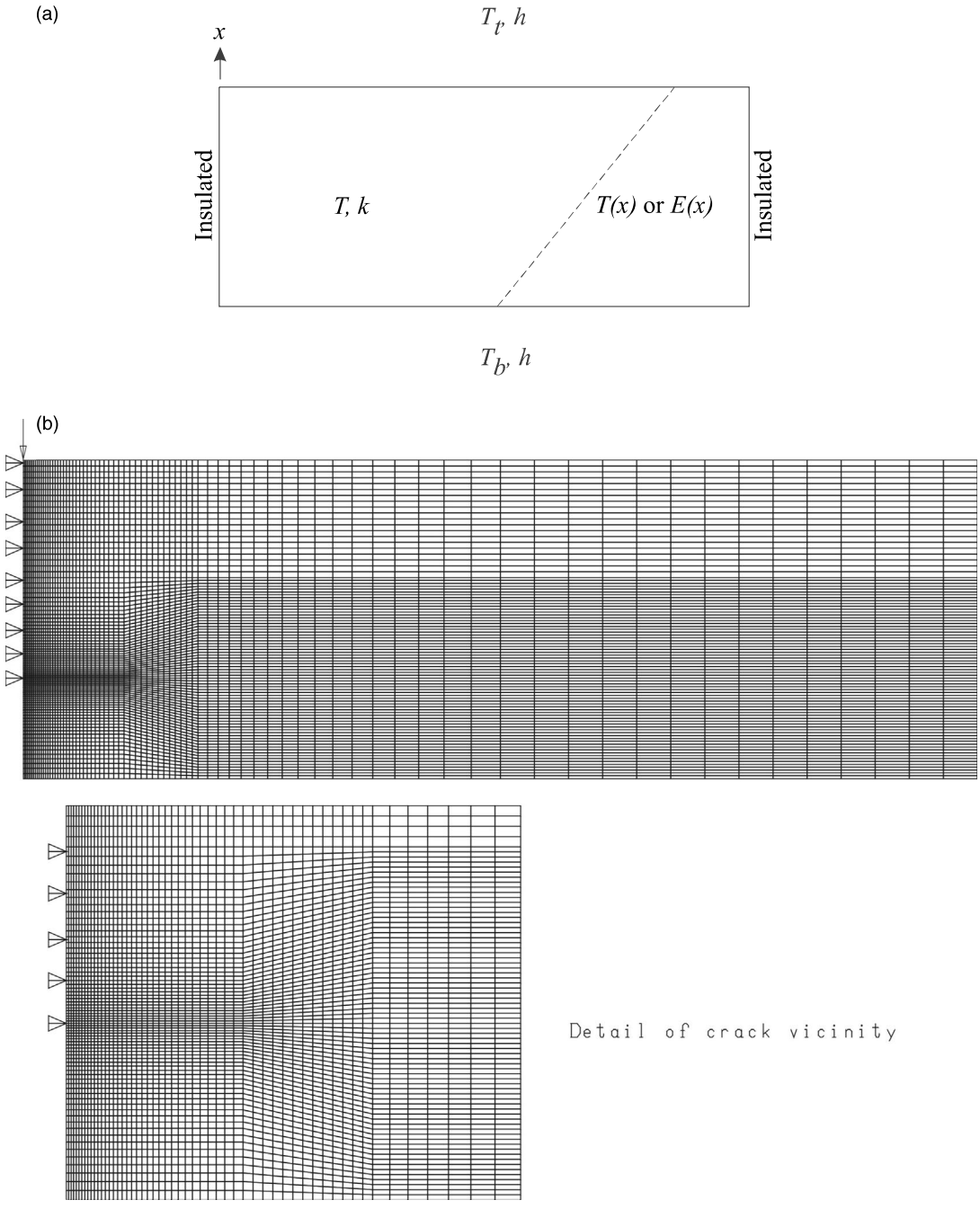

Fig. 2. Numerical model: (a) thermomechanical analysis to apply Young's modulus variation, (b) finite element discretization.

Several methods are available for extracting of crack tip SIFs from numerical models of FGMs. A modified path independent integral J^* has been successfully implemented by Eischen (1987) and by the authors (Rousseau, 2000) who have recorded differences of less than 2% with available static solutions

(Erdogan, 1995) in statically loaded cracked FGM beams. The crack closure integral, widely used in homogeneous cracked bodies, can potentially be used in FGMs as well. Evaluating crack tip SIFs from the numerical models through regression analysis of computed crack tip opening displacements was also found to offer similar accuracy (Rousseau, 2000). In fact, the method has been successfully adopted earlier by Marur and Tippur (2000) and Rousseau and Tippur (2000a) to determine dynamic and static SIFs, respectively, in FGMs with cracks perpendicular to the elastic gradient direction. Accordingly, it is used here to retrieve instantaneous crack tip SIFs in FGMs because of its simplicity. In this method, values of crack opening displacements in the immediate vicinity of the crack tip only are used. Hence, K-dominant assumptions are reasonable. Therefore, crack opening displacement relates to SIF as follows:

$$\delta_y(t)\big|_{\theta=\pm\pi, r\to 0} = \frac{8\bar{K}_{\mathrm{Id}}(t)}{E_0}\sqrt{\frac{r}{2\pi}}. \tag{4}$$

As discussed earlier, this equation is valid for both homogeneous materials and FGMs. In the latter case, E_0 denotes the crack tip Young's modulus. Variations of $\bar{K}_{\mathrm{Id}}\ (r, \pm\pi)$ obtained from the finite element solution are plotted and the extrapolated value to the crack tip is the SIF being sought,

$$|K_{\mathrm{Id}}| = \lim_{r\to 0}|\bar{K}_{\mathrm{Id}}|. \tag{5}$$

A typical plot of $\bar{K}_{\mathrm{Id}}\ (r, \pm\pi)$ variation and determination of the crack tip value of the same is shown in Fig. 3. Also, plots of $\ln(\delta_y)$ vs. $\ln(r)$ (not presented) for homogeneous materials and FGM show a slope of $1/2$, further confirming the inverse square root singularity in FGMs.

3.1. Verification of the finite element model

Reliability of the finite element model and the adopted methodology were first checked. Due to the lack of closed-form solutions for dynamically loaded FGMs at the moment, SIF histories from finite element analysis were compared with the ones reported in Mason et al. (1992) for homogeneous bodies. In that

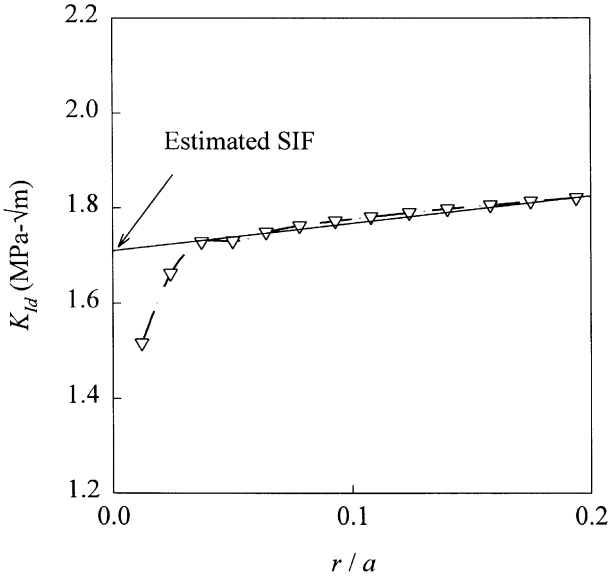

Fig. 3. Evaluation of dynamic SIF from FEA using regression analysis of crack opening displacements.

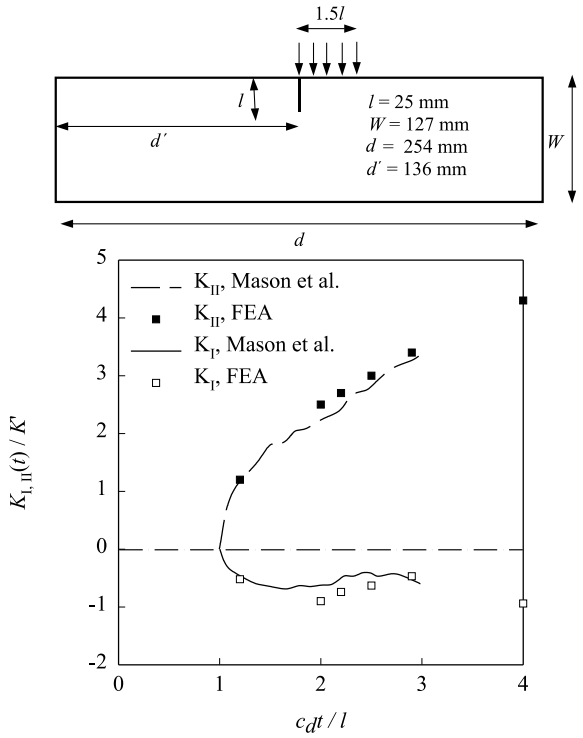

Fig. 4. Normalized SIF as a function of normalized time for asymmetrically impacted cracked PMMA beam.

work, FEA results for an asymmetrically and dynamically loaded cracked PMMA beam (see, inset in Fig. 4) are reported. It should be noted, however, that in that example crack tip experiences mixed-mode loading and hence both K_I and K_{II} histories are to be evaluated. In doing so, counterparts of Eqs. (4) and (5) for calculating K_{II} using crack sliding displacements are also required along with the ones for K_I. Using the methodology outlined in the preceding paragraph, SIFs at different instances of time were calculated and compared. Good agreement is observed for both mode-I and mode-II SIFs shown in Fig. 4.

It should also be noted that numerically determined SIFs for FGM beams loaded *statically* using the proposed methodology were found to be in agreement to well within 10% of the optical measurements reported elsewhere (Rousseau, 2000; Rousseau and Tippur, 2000a) and further supports the adopted numerical procedure.

Next, an example of the SIF history computed using the above method is presented for an FGM with $E_2/E_1 > 1$. Only essential details on material characteristics and experiments are included here for brevity and details can be found in Rousseau and Tippur (2001b). The dimensions of the FGM beam used in the experiment and numerical simulation were 152 mm × 37 mm × 6 mm. The experimentally determined variation of Young's modulus and density over the height of the beam (X-direction in Fig. 1) are shown in Fig. 5(a). The corresponding spatial variation in E/ρ along the height of the beam is shown in Fig. 5(b). The finite element analysis simulated low velocity symmetric one point impact of 5.3 m/s as in the experiments. The solid line in Fig. 5(c) shows computed dynamic SIF history. Experimental values, shown as open symbols, were obtained using the optical method of coherent gradient sensing (CGS) (Tippur et al., 1991). The optical measurements were subjected to overdeterministic least-squares analysis using asymptotic equations for dynamically loaded stationary cracks for extracting SIFs. In Fig. 5(c) the results up to crack

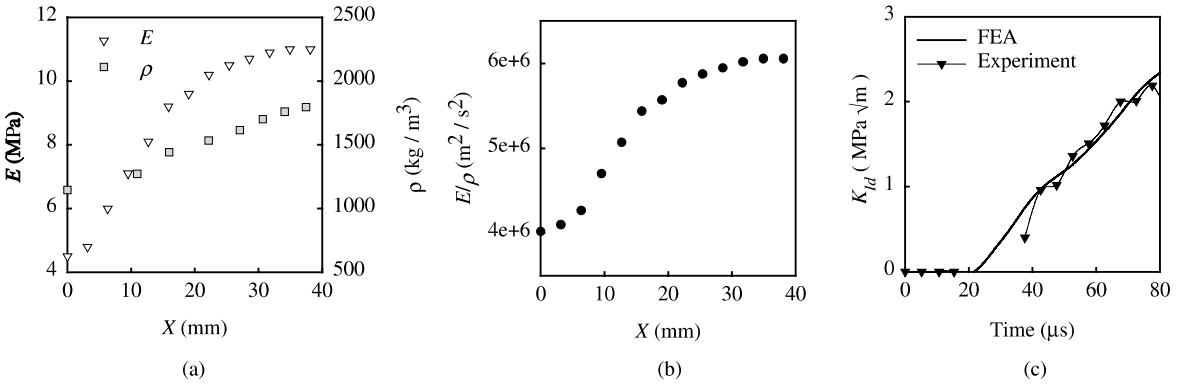

Fig. 5. Dynamic SIF history (c) for FGM shown in (a) and (b).

initiation, at about 90 μs in this case, are shown. Remarkably good agreement exists between numerical and experimental results. A SIF of ~2.6 MPa $\sqrt{m}$ is measured at crack initiation. This value represents the crack initiation toughness of the material at the crack tip location and was further verified independently by fracture toughness tests on homogeneous glass-filled epoxy specimens with volume fraction of the filler equal to that at the crack tip of the FGM.

4. Hypothetical material property variations

A series of finite element simulations on homogeneous and FGM beams with assumed material property variations were performed to determine the type of the elastic gradient that would be desirable from the stand point of fracture initiation. The simulations were guided by experimental works by the authors (Rousseau and Tippur, 2001b) on glass-filled epoxy FGM. That is, elastic material properties were kept within the range of those realized in the actual glass/epoxy FGM. Accordingly, Young's moduli were varied between 4 and 12 GPa, and densities between 950 and 1850 kg/m^3. Thus, elastic modulus ratio of 3:1 corresponds to a ratio E/ρ of 1.5:1 (6.5×10^6–4.2×10^6 m^2/s^2). Simulated geometries were set to dimensions 160 mm × 40 mm × 5 mm ($l \times W \times B$), with a crack length of $a/W = 0.2$.

In this study, material variations were identified in terms of E/ρ variations and Poisson's ratio was kept constant ($v = 0.34$). Different power-law descriptions of E/ρ between the terminal values of 6.5×10^6 and 4.2×10^6 m^2/s^2 were described. Individual variations of E and ρ were implemented using a 'look-up' chart that relates E, ρ, (and E/ρ) to filler volume fraction in actual glass-filled epoxy. Two sets of numerical simulations were conducted: (a) the first consisted of identical E/ρ ratios between the top and bottom edges of the beam with different power-law descriptions of the variations and, (b) the second were with linear variations of increasing, decreasing values of E/ρ for FGMs, and constant E/ρ representing homogeneous materials, all having identical E/ρ at the crack tip. Further, the variations in E/ρ were expressed by a power-law function,

$$\frac{E(X)}{\rho(X)} = \left(\frac{E}{\rho}\right)_1 + \left\{\Delta\left(\frac{E}{\rho}\right)\right\}\left(\frac{X}{W}\right)^n,$$

where X is the distance from the bottom edge of the beam, subscripts 1 or 2 represent values at the bottom or top edge of the beam, respectively, and $\Delta(E/\rho)$ represents the difference between the values at the bottom

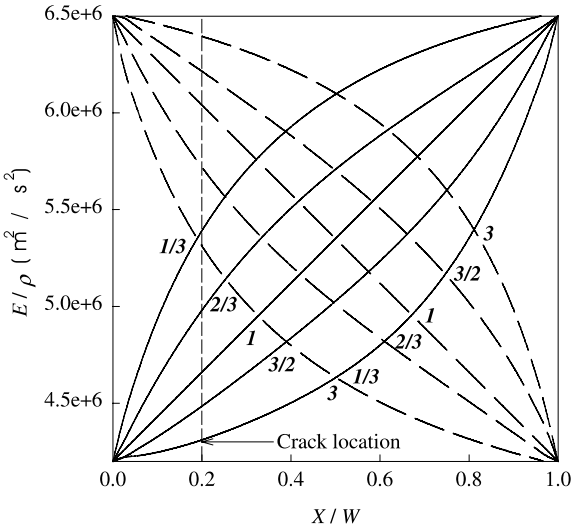

Fig. 6. Elastic profiles used in finite element simulations (gradation exponent n is shown for each curve) ($a/W = 0.2$).

and at the top edges. Knowing, E/ρ variation with volume fraction of solid-glass filler in epoxy matrix from a previous experimental work (Rousseau and Tippur, 2001b), individual spatial variations of E and ρ were determined for finite element implementation.

The E/ρ variations for values of the exponent $n = 1/3$, $2/3$, 1, $3/2$, and 3 are shown in Fig. 6. For an FGM with an increasing elastic gradient ($n \equiv n^{\mathrm{i}}$), the average value $((E/\rho)_{\mathrm{avg}} = (1/W)\int_0^W [E(X)/\rho(X)]\,\mathrm{d}X)$ of elastic modulus increases as n decreases. Conversely, for a decreasing elastic gradient ($n \equiv n^{\mathrm{d}}$), the material has higher integrated average Young's modulus to density ratio, $(E/\rho)_{\mathrm{avg}}$, as n increases. As indicated in the figure, the crack tip in each case is located at $X/W = 0.2$ ($a/W = 0.2$). Therefore, curves with exponent $n = 3$, for both increasing and decreasing FGM gradients, represent cases where the entire crack resides nearly in a homogeneous medium, with the uncracked ligament having a relatively steep gradient. On the other hand, curves with gradation coefficient $n = 1/3$, for both increasing and decreasing FGM gradients, have cracks located in regions of very rapid gradients, with the impact locations being nearly homogeneous.

The second set of numerical evaluation was performed to complement the first. It was aimed at determining which one of a homogeneous, or FGM beams with linearly increasing or decreasing gradients, all with the same crack tip material properties, would show favorable SIF history. Equal crack tip properties were achieved in each case by setting the crack length to $a/W = 0.5$. Further, it should be noted that here the average values of longitudinal and shear wave speeds of the three cases are identical and facilitate isolating the elastic gradient effects on fracture parameters.

5. Influence of material property gradients on dynamic impact

5.1. Effect of gradient profile

In each case at $t = 0$, low velocity impact occurred at $X/W = 1$. In beams with $E_2/E_1 > 1$, the compressive stress waves generated at the impact point progressively encounter relatively more compliant

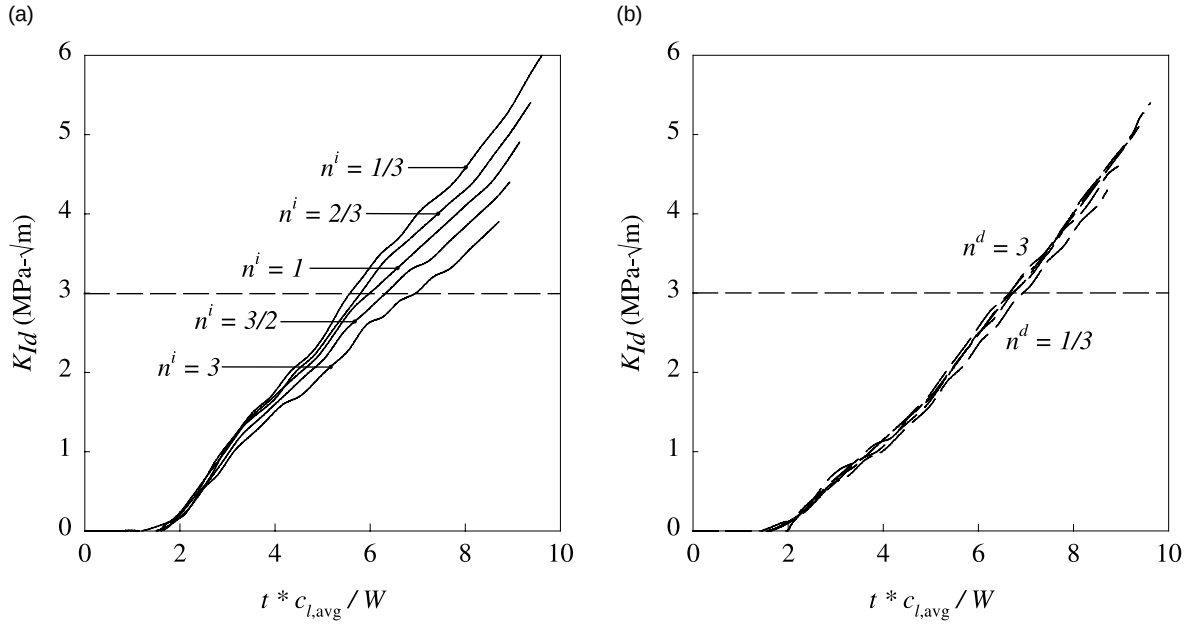

Fig. 7. SIF variation in FGMs with (a) increasing, and (b) decreasing gradient profiles.

material and hence waves decelerate as they move away from the impact edge (in $-X$ direction) towards the crack. The opposite occurs in FGMs with $E_2/E_1 < 1$; that is, compressive waves progressively encounter relatively stiffer material as they propagate away from the top edge of the beam and hence accelerate towards the cracked edge. The reflected tensile waves in the two cases accelerate and decelerate, respectively. These would have distinct influence on the evolution of crack tip stresses and hence the fracture parameters. Fig. 7(a) and (b) show the evolution of K_{Id} with time for progressively increasing and decreasing values of E/ρ ahead of the crack tip. For subsequent analyses, time is normalized with respect to the average dilatational wave speed of the FGM and the specimen height: $T = t^* C_{l,\text{avg}}/W$, where $C_{l,\text{avg}} = (1/W)\int_0^W C_l(X)\,\mathrm{d}X$. In all cases, significant values of K_{Id} are observed only beyond $T \sim 1.5$, after the reflected tensile waves reach the crack tip, and are followed by monotonic increase in stress intensification. FGMs with increasing gradients have noticeable spreads in their variation when compared to the ones with the decreasing gradients which are narrowly banded for the same temporal resolution. This indicates that the effect of the gradient profile on FGMs with $E_2/E_1 < 1$ is relatively small when compared to those with $E_2/E_1 > 1$. Also, within each category, FGMs with lower average values E/ρ, and hence lower average stress wave speeds, have smaller increasing rates of SIFs than their counterparts with higher elastic properties. Variations in K_{Id} for both increasing and decreasing gradients are non-uniform and show oscillations throughout the events. These oscillations are attributed to discrete wave reflections from the edges that occur in finite configurations. The $K_{\text{Id}}(t)$ values monotonically increase after approximately $T \sim 1.5$. All FGMs with increasing gradients show a somewhat linear increase while the ones with decreasing gradients show nonlinearity characterized partly by lower initial crack tip loading rate.

Rates of increases in K_{Id} for the terminal values of n of each case (Fig. 6) are shown in Fig. 8. These were obtained by direct forward difference estimation as $\Delta K_{\text{Id}}/\Delta t$. As can be surmised from Fig. 7, higher overall elastic properties result in steeper rate of increase in K_{Id}. For decreasing gradients (broken lines in Fig. 8), monotonic increase in $K_{\text{Id}}/\Delta t$ is evident during the observation window. On the contrary, for increasing gradients (solid lines in Fig. 8), $\Delta K_{\text{Id}}/\Delta t$ values are initially higher than the ones for the decreasing gradients

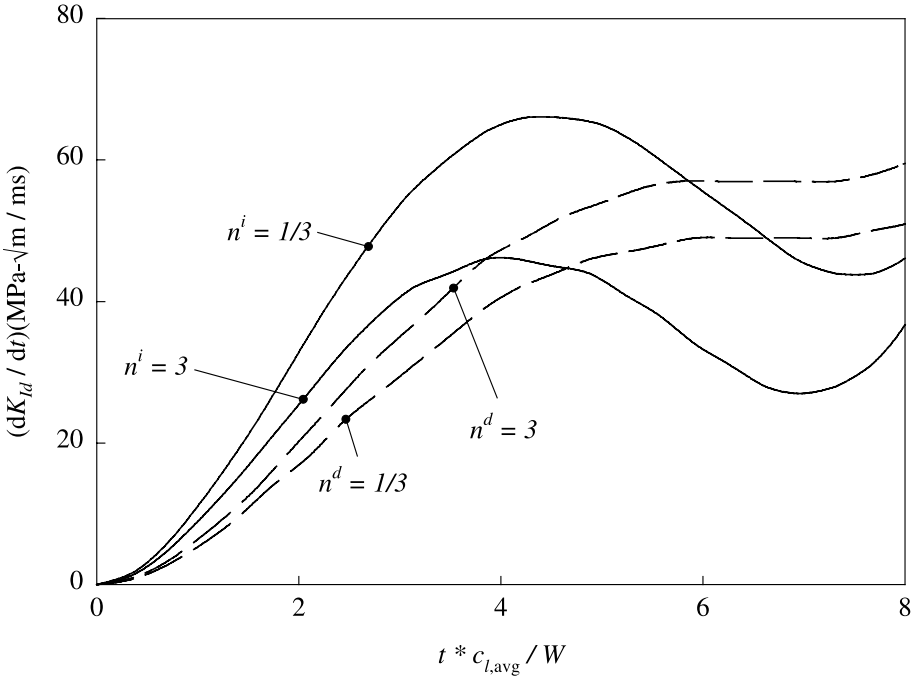

Fig. 8. Rate of increase in SIF in FGMs for select elastic gradient profiles.

and monotonically increase up to about $T \sim 4$. Beyond that point, they decrease to values below the ones for the decreasing gradients.

Next, the effect of the elastic gradient profile on the dynamic fracture initiation of the FGM is examined. For the purpose of this evaluation, it is assumed that the crack would initiate when the crack tip K_{Id}, reaches, say, 3 MPa $\sqrt{\mathrm{m}}$, which is the average dynamic crack initiation toughness of the glass-filled epoxy used in the experiments. The results are shown in Fig. 9 for increasing and decreasing gradients. For both types of gradients, the trend is one of earlier crack initiation in those with higher average value of E/ρ. Note however, that for decreasing gradients, the difference is only marginal and initiation time is nearly constant within the accuracy of K_{Id} evaluation. The following general conclusions can thus be reached: Lower average values of E/ρ (or, lower average value of wave speeds) ($n^{\mathrm{d}} = 1/3$, $n^{\mathrm{i}} = 3$) delay crack initiation. In addition, generally crack initiation is delayed for decreasing elastic properties ahead of the crack than for increasing ones. Consequently, cracks situated on the stiff side of an FGM are more favorable than if located on the compliant side of the FGM. Interestingly, this is true only under dynamic conditions since the opposite is found under quasi-static conditions (Rousseau and Tippur, 2001a), where the crack tip on the compliant side is elastically shielded when compared to the one on the stiff side for identical far field symmetric loading conditions.

As stated earlier, the intent of the paper is to isolate the effects of elastic gradients on crack initiation in FGMs. Hence, the crack initiation times only reflect the effect of elastic gradients. However, it should be emphasized that FGMs are generally produced by introducing compositional/microstructural gradients. Hence, introducing elastic property gradients alone while keeping the fracture toughness constant, as done in the above idealized simulations is conceivable but could be challenging. Accordingly, for completeness, the combined influence of elastic gradients and dynamic crack initiation toughness for the specific case of nominally brittle glass-filled epoxy FGMs is included in Appendix A.

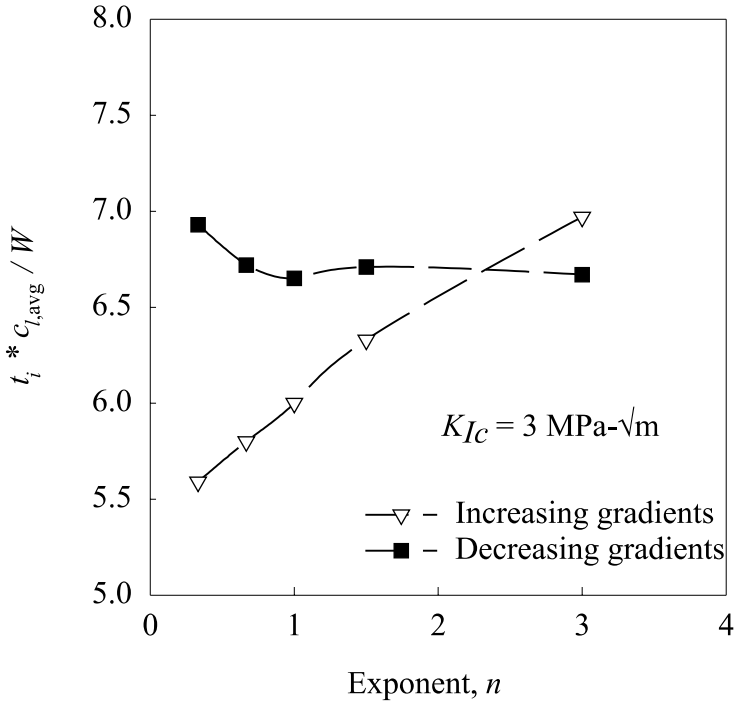

Fig. 9. Crack initiation times in cracked FGM with increasing, and decreasing gradient profiles.

5.2. Effect of elastic gradient direction

In the previous set of simulations, the combined effect of the average value of wave speeds in each beam, crack tip elastic modulus and crack tip elastic gradients ($\mathrm{d}E/\mathrm{d}X$) are responsible for the differences in the crack initiation time and $\Delta K_{\mathrm{Id}}/\Delta t$ variations. Accordingly simulations to isolate the effect of increasing and decreasing elastic gradients was undertaken. Plot of K_{Id} variation with time after impact is shown in Fig. 10(b) for the three elastic variations, all having identical average elastic properties and crack tip properties ($a/W = 0.5$), depicted in Fig. 10(a). The variation in SIF for the FGM with $E_2/E_1 > 1$ displays the steepest rate of increase whereas the FGM with $E_2/E_1 < 1$ has the lowest rate of increase. The homogeneous material response lies in between the two FGMs, though slightly closer to the FGM with $E_2/E_1 > 1$. Rates of increase in $\mathrm{d}K_{\mathrm{Id}}/\mathrm{d}t$ (Fig. 11) are again lowest for FGM with $E_2/E_1 < 1$, followed by the homogeneous material. The FGM with $E_2/E_1 > 1$ has the steepest increase up to $T \sim 5$. Beyond that point, an inflection in the curve drops the increase in stress intensification below that of the homogeneous material.

With the idealization that crack initiation occurs at a constant K_{Id} in all the three cases, crack initiation times can also be determined directly from Fig. 12 as 5.8, 6.6, and 7.9 for cases of FGMs with increasing gradient, homogeneous material, and FGMs with decreasing gradient, respectively, for an assumed critical value of, say, 3 MPa $\sqrt{\mathrm{m}}$. Thus, purely based on elastic considerations, crack initiation in the latter case is significantly delayed, by a factor of ~1.4, when compared to the former. Behavior of the homogeneous material, as with all other parameters, lies between the two FGMs.

To understand these differences in fracture behavior, dynamic impact simulations on *uncracked* beams were performed for monitoring stress histories. Contours ($\sigma_x + \sigma_y$) for all three materials are shown in Fig. 13 after several wave reflections ($T = 5.7$) between the top and bottom edges. Relative to the homogeneous

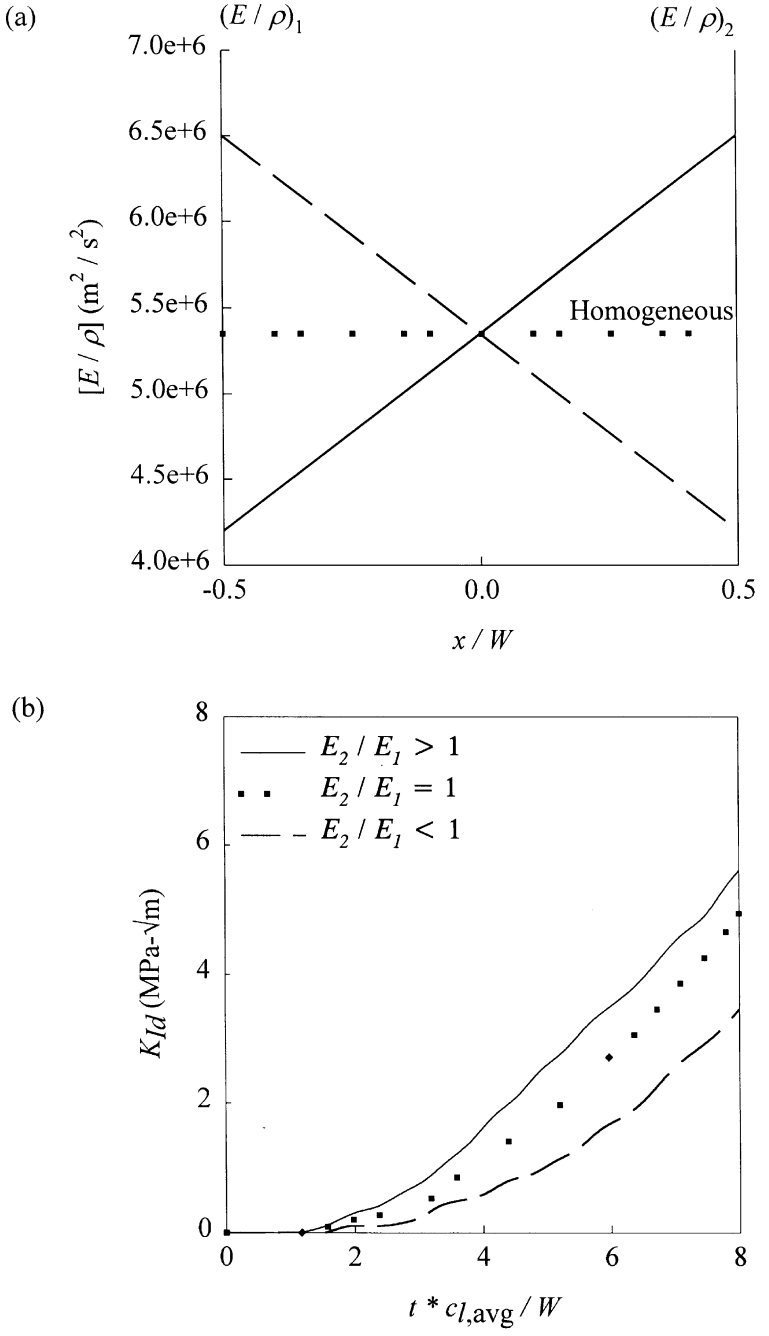

Fig. 10. SIF history in homogeneous beams and FGMs with linearly varying gradients (crack tip located at $X/W = 0.5$ or $X/W = 0$).

beam (Fig. 13(b)), compressive waves emanating from the impact point for the FGM with $E_2/E_1 > 1$ are constricted vertically, whereas those for the FGM with $E_2/E_1 < 1$ are elongated in the same direction. In the former case, as these compressive waves (for example, contour level D in Fig. 13) travel from the top to

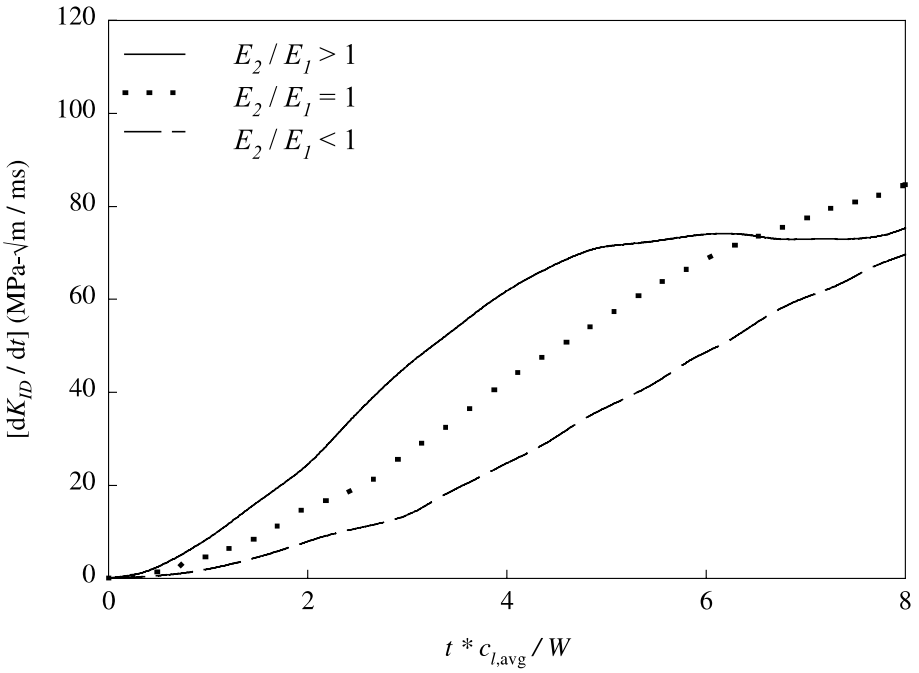

Fig. 11. Rate of increase in SIF history for homogeneous beams and FGMs with linearly varying gradients.

the bottom edge, they are delayed by material property variations in that direction. Conversely, for the FGM with $E_2/E_1 < 1$, material property variation promotes faster wave propagation downwards, thereby elongation of $(\sigma_x + \sigma_y)$ contour (again, level D) along the beam height is evident. The reflected tensile waves accelerate upward for FGMs with $E_2/E_1 > 1$, decelerate for FGMs with $E_2/E_1 < 1$, and propagate at a constant speed in the homogeneous case. As seen in Fig. 13, at time $T = 5.7$, a point P (located at $X/W = 0.5$) along the line of symmetry of the beam experiences tensile stresses for the FGM with $E_2/E_1 > 1$ while the corresponding points in the homogeneous beam and the FGM beam with $E_2/E_1 < 1$ experience progressively higher compressive stresses, respectively. Accordingly, the latter two cases are elastically shielded from tensile stresses for a longer duration and would experience failure at a later time.

6. Conclusions

The dynamic response of homogeneous beams and FGMs with cracks parallel to the elastic gradient, under low velocity impact was evaluated numerically using finite element analysis. The material nonhomogeneity was described by power-law variation of E/ρ ratios with increasing and decreasing elastic gradient profiles defined in terms of gradation exponent varying from 1/3 to 3. In each case, dynamic SIF history was determined. Elastic gradient effects were isolated and fracture performance of each FGM is evaluated in terms of time needed for crack initiation and rate of crack tip loading. Results indicate that the gradient profiles have relatively less effect when the crack is situated on the stiff side of the gradient with impact occurring on the compliant side than for the opposite configuration. The computations demonstrate that FGMs with cracks on the stiff side of the gradient generally show much lower rate of crack tip loading and hence delayed crack initiation when compared to homogeneous materials or FGMs with cracks on the

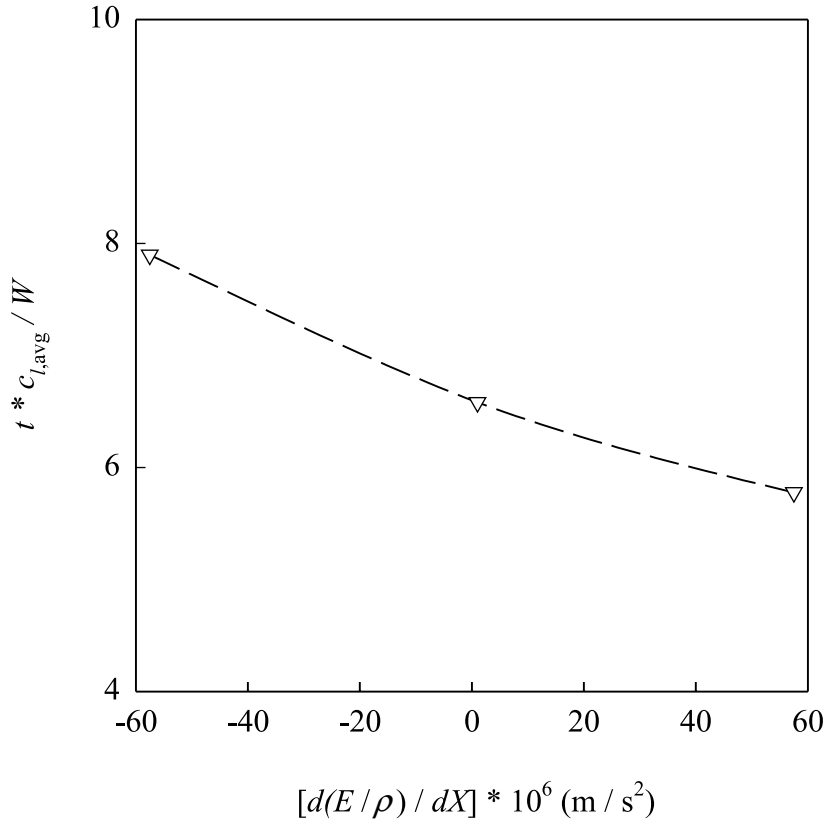

Fig. 12. Time at initiation for homogeneous beams and FGMs with linearly varying gradients.

compliant side of the gradient. The observations are explained by examining stress histories in uncracked beams of identical nonhomogeneity subjected to identical loading.

Acknowledgements

The support of this research by NSF Materials Program (CMS-9622055) and ARO Solid Mechanics Program (DAAG55-97-0110) is gratefully acknowledged.

Appendix A

FGMs are generally produced by spatially grading the microstructure and/or morphology of the constituents. Thus, in a typical FGM both elastic properties and failure characteristics (say, strength, fracture toughness) may vary spatially. Hence, the example of glass-filled epoxy (solid sphere glass filler ~40 μm mean diameter in a slow curing epoxy), studied Rousseau (2000), is considered to examine the combined effect of elastic and fracture toughness gradients on crack initiation in FGM beams subjected to impact loading as done in Section 4. In Fig. 14(a), measured elastic wave propagation speeds (proportional to $\sqrt{E/\rho}$) in glass-filled epoxy for different volume fraction are shown. These elastic wave speed measurements were performed using ultrasonic pulse echo measurements as reported in Butcher et al. (1999). The

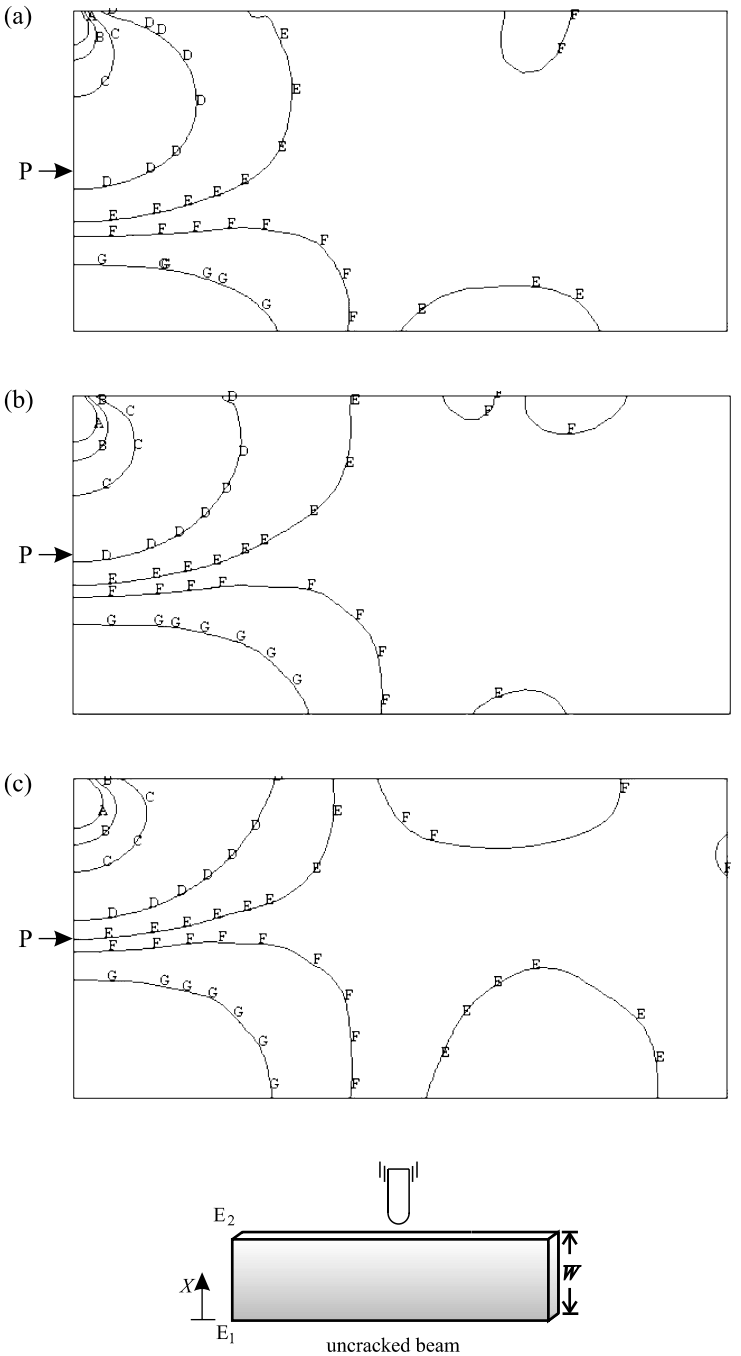

Fig. 13. ($\sigma_x + \sigma_y$) contours at non-dimensional time $T = 5.7$. (A = −5, B = −3.5, C = −2, D = −0.5, E = −0.1, F = 0.1, G = 0.5) 10 MPa. (a) $E_2/E_1 < 1$, (b) $E_2/E_1 = 1$, (c) $E_2/E_1 > 1$. Point P corresponds to ($X/W = 0.5$, $y = 0$). Note that only the right-half of the beam is modeled.

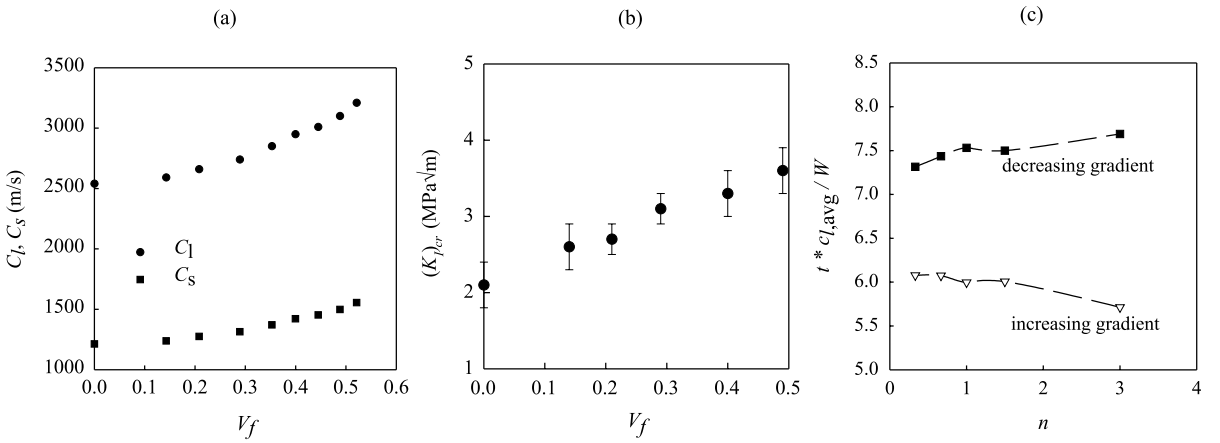

Fig. 14. Dynamic material properties of glass-filled epoxy and time for crack initiation. (a,b) Variation of elastic properties and dynamic crack initiation toughness with filler volume fraction, (c) crack initiation time for different elastic gradients shown in Fig. (5).

variation in the crack initiation toughness values for the same material at different volume fractions of the filler is shown in Fig. 14(b). These were obtained separately from impact experiments conducted in an instrumented Instron-Dynatup drop tower with an impact velocity of 1.5 m/s. The samples were single edge cracked (sharp cracks) beams loaded in three-point bending configuration. The maximum load registered by the tup was used for determining the crack initiation toughness.

Using the data in Fig. 14(a,b) in conjunction with the elastic variations shown in Fig. 5, time for crack initiation in the two sets of FGMs with increasing and decreasing elastic gradients were computed by finite element analysis described in Sections 3 and 4. As before, simulations consisted of symmetric one-point impact loading of FGMs on the edge of the beam opposing the cracked edge. The times for crack initiation in FGMs, thus obtained, with increasing and decreasing gradients are shown in Fig. 14(c). Evidently, the trend is one of earlier crack initiation in FGMs with crack residing on the compliant side of the beam and increasing elastic gradient ahead of the crack when compared to those with crack on the stiff side with decreasing elastic gradient ahead of the crack. (This is similar to the earlier observation made in the context of Fig. 9 where elastic effects alone were isolated and studied.) Apart from that, within the accuracy of measurements, the combined effect of elastic gradients and crack initiation toughness (for this material) on time for crack initiation is rather benign in both increasing and decreasing elastic gradient.

References

Babaei, R., Lukasiewicz, S.A., 1998. Dynamic response of a crack in a functionally graded material between two dissimilar half-planes under anti-plane shear impact load. Engineering Fracture Mechanics 60 (4), 479–487.

Butcher, R.J., Rousseau, C.-E., Tippur, H.V., 1999. Functionally graded particulate composite: preparation, measurements and failure Analysis, Acta Materialia 47, 259–268.

Chiu, T.-C., Erdogan, F., 1999. One dimensional wave propagation in functionally graded elastic medium. Journal of Sound and Vibration 222 (3), 453–487.

Delale, F., Erdogan, F., 1983. The crack problem for a non-homogeneous plane. ASME Journal of Applied Mechanics 50, 609–614.

Eischen, J.W., 1987. Fracture of non-homogeneous materials. International Journal of Fracture 34, 3–22.

Erdogan, F., 1995. Fracture mechanics of functionally graded materials. Composites Engineering 7, 753–770.

Gu, P., Dao, M., Asaro, R.J., 1999. A simplified method for calculating the crack-tip field of functionally graded materials using the domain integral. Journal of Applied Mechanics 66, 101–108.

Jin, Z.-H., Noda, N., 1994. Crack-tip singular fields in non-homogeneous materials. ASME Journal of Applied Mechanics 61, 738–740.

Kim, A.S., Suresh, S., Shih, C.F., 1997. Plasticity effects on fracture normal to interfaces with homogeneous and graded compositions. International Journal of Solids and Structures 34 (26), 3415–3432.

Li, H., Lambros, J., Cheeseman, B., Santare, M.H., 1999. Experimental investigation of quasi-static fracture of functionally graded material. International Journal of Solids and Structures 37 (27), 3715–3732.

Marur, P.R., Tippur, H.V., 2000. Dynamic response of bimaterial and graded interface cracks under impact loading. International Journal of Fracture 103, 103–109.

Mason, J.J., Lambros, J., Rosakis, A.J., 1992. The use of a coherent gradient sensor in dynamic mixed-mode fracture mechanics experiments. Journal of the Mechanics and Physics of Solids 40 (3), 641–661.

Nakagaki, M., Wu, Y.D., Hagihara, S., 1998. Dynamically propagating crack in graded particle dispersed composites. Fracture and Strength of Solids 145, 333–342.

Parameswaran, V., Shukla, A., 1998. Dynamic fracture of a functionally gradient material having discrete property variation. Journal of Materials Science 33, 3303–3311.

Parameswaran, V., Shukla, A., 1999. Crack-tip stress fields for dynamic fracture in functionally gradient materials. Mechanics of Materials 31, 579–596.

Rousseau, C.-E., 2000. Evaluation of crack tip fields and fracture parameters in functionally graded materials. Ph.D. Dissertation, Auburn University.

Rousseau, C.-E., Tippur, H.V., 2000a. Compositionally graded materials with cracks normal to the elastic gradient. Acta Materialia 48, 4021–4033.

Rousseau, C.-E., Tippur, H.V., 2001a. Evaluation of crack tip fields and stress intensity factors in functionally graded elastic materials: crack parallel to elastic gradient. Submitted for publication.

Rousseau, C.-E., Tippur, H.V., 2001b. Dynamic fracture of compositionally graded materials with cracks along the elastic gradient: experiments and analysis. Mechanics of Materials, in press.

Tippur, H.V., Krishnaswamy, S., Rosakis, A.J., 1991. A coherent gradient sensor for crack tip deformation measurements: analysis and experimental results. International Journal of Fracture 48, 193–204.

Tohgo, K., Sakaguchi, M., Ishii, H., 1996. Applicability of fracture mechanics in strength evaluation of functionally graded materials. JSME International Journal – Series A 39 (4), 479–488.